HHS Public Access

Author manuscript

Dev Biol. Author manuscript; available in PMC 2022 November 10.

Published in final edited form as:

Dev Biol. 2022 October ; 490: 1–12. doi:10.1016/j.ydbio.2022.06.014.

Independent pathways control muscle tissue size and sarcomere remodeling

David Brooks,

Simranjot Bawa,

Alexandria Bontrager,

Marta Stetsiv,

Yungui Guo,

Erika R. Geisbrecht*

Department of Biochemistry and Molecular Biophysics, Kansas State University, Manhattan, KS, 66506, USA

Abstract

Cell growth and proliferation must be balanced during development to attain a final adult size with the appropriate proportions of internal organs to maximize fitness and reproduction. While multiple signaling pathways coordinate *Drosophila* development, it is unclear how multi-organ communication within and between tissues converge to regulate systemic growth. One such growth pathway, mediated by insulin-like peptides that bind to and activate the insulin receptor in multiple target tissues, is a primary mediator of organismal size. Here we uncover a signaling role for the NUAK serine/threonine kinase in muscle tissue that impinges upon insulin pathway activity to limit overall body size, including a reduction in the growth of individual organs. In skeletal muscle tissue, manipulation of NUAK or insulin pathway components influences sarcomere number concomitant with modulation of thin and thick filament lengths, possibly by modulating the localization of Lasp, a nebulin repeat protein known to set thin filament length. This mode of sarcomere remodeling does not occur in other mutants that also exhibit smaller muscles, suggesting that a sensing mechanism exists in muscle tissue to regulate sarcomere growth that is independent of tissue size control.

Keywords

NUAK; *Drosophila* ; Muscle; Sarcomere; Insulin signaling

1. Introduction

Both extrinsic and intrinsic influences contribute to the regulation of organismal body size. External factors such as increased temperature, low oxygen levels, and limited

*Corresponding author. geisbrechte@ksu.edu (E.R. Geisbrecht).

Appendix A. Supplementary data

Supplementary data to this article can be found online at https://doi.org/10.1016/j.ydbio.2022.06.014.

nutrient availability reduce organismal growth, while internal factors like genetic diversity and intertissue communication occur within organisms and may vary among individuals (Koyama et al., 2013, 2020; Mirth and Shingleton, 2012; Texada et al., 2020). The *Drosophila* model is particularly amenable to the study of body size control due its fast life cycle, conserved signaling pathways that regulate growth, and genetic tools for inducing changes in one tissue and analyzing outputs in another (Droujinine and Perrimon, 2016; Koyama et al., 2020).

Multiple growth regulatory pathways coordinate *Drosophila* tissue and systemic growth during development (Texada et al., 2020). The Target of Rapamycin (Tor) pathway senses nutrients in a cell-autonomous manner, while circulating levels of steroids and insulin-like peptides are the main regulatory factors that contribute to systemic growth (Koyama et al., 2013; Mirth and Shingleton, 2012; Texada et al., 2020). Ecdysone is the main steroid hormone that binds to the heterodimeric receptor complex composed of the ecdysone receptor (EcR) and Ultraspiracle (Usp) to regulate target gene expression (Hu et al., 2003; Schwedes and Carney, 2012; Yao et al., 1992). Insulin receptors respond to insulin/insulin-like peptides and transmit downstream events primarily through the phosphorylation of Akt, which promotes protein synthesis and inhibits activity of the transcription factor FOXO (Biglou et al., 2021; Garofalo, 2002; Nässel et al., 2015). In well fed larvae, phosphorylated FOXO is excluded from the nucleus and growth is allowed to proceed (Jünger et al., 2003; Kramer et al., 2003; Puig et al., 2003). Nutrient deprivation or low insulin pathway activity derepresses FOXO, which promotes gene expression through the action of 4EBP to slow down and/or inhibit growth (Jünger et al., 2003; Puig et al., 2003). Despite these seemingly simple signal transduction pathways, complex intracellular and intertissue interactions between these and other signaling pathways coordinate growth during larval development. Insulin signaling is coupled to nutrient availability through the Tor pathway at the cellular level, while antagonistic relationships between the insulin and ecdysone endocrine axes at the organismal level mediate systemic growth (Koyama et al., 2020; Texada et al., 2020).

Final adult size is dependent on the rate and duration of larval growth in *Drosophila*. A checkpoint in early third larval instar (L3) development called critical weight (CW) ensures nutrient availability. Failure to reach CW results in a delay of imaginal disc patterning, as well as the transition through metamorphosis (Beadle et al., 1938; Mirth et al., 2005; Shingleton et al., 2005; Stieper et al., 2008). Systemic suppression of the insulin pathway causes these same developmental delays, supporting the importance of insulin dependence on growth processes required for attaining critical weight (Koyama et al., 2013; Mirth and Shingleton, 2012). One interesting feature in the determination of organismal size is the proportional scaling of tissues and organs during growth, largely mediated by insulin signaling (Koyama et al., 2020; Texada et al., 2020). While the Activin branch of the TGFβ signaling network acts upstream and promotes insulin signaling in *Drosophila* skeletal muscle tissue, Activinβ (Actβ) disproportionally limits the growth of skeletal muscle relative to other tissues (Moss-Taylor et al., 2019). These data suggest that control of final muscle size is regulated independently and not coordinately scaled with the growth of other organs during development.

Much less is understood about the geometric control of muscle growth, which can occur in three dimensions. Rather than simply an increase in the production of proteins, skeletal muscle growth is largely characterized by the addition of proteins into ordered arrays of repeating sarcomeres (Gautel and Djinović-Carugo, 2016; Jorgenson et al., 2020). Sarcomeres comprise the smallest unit capable of contraction within muscle tissue and can be added in series to increase the length of a myofiber. Sarcomeric proteins are also added to existing sarcomeres in other directions to increase the width and/or the thickness of a muscle cell. While it is well established that chronic stretching or muscle disuse can influence serial sarcomere addition or subtraction (Jorgenson et al., 2020), specific signaling pathways that contribute to alterations in sarcomere number and/or size are surprisingly understudied. A 2010 report showed that the addition of insulin growth factor-1 (IGF-1) to isolated mouse myofibers induced the localization of N-Wasp for unbranched actin filament formation (Takano et al., 2010). Recent data shows that Actβ acts upstream of the insulin pathway to regulate muscle width and thickness in *Drosophila* larval muscles (Kim and O'Connor, 2021).

Here we show that muscle-specific overexpression of the evolutionarily conserved serine/threonine kinase NUAK reduces organismal size and a concomitant decrease in the growth of all tissues, including skeletal muscle. Excess NUAK also blocks muscle insulin signaling and surprisingly causes alterations in sarcomere number and length. In light of the findings that other genotypes with smaller muscles do not change sarcomere parameters, we propose that a sensing mechanism exists in muscle tissue to regulate sarcomere growth that is independent of tissue size control.

2. Materials and methods

2.1. Drosophila genetics

Fly lines were kept on standard cornmeal-yeast-agar medium at 25 °C unless noted. *P(EPgy2)NuakEY22355* (BL22554) is an insertion in the *NUAK* locus that drives UAS-based expression (UAS-*NUAK EY*). Generation of UAS-*NUAK K99R* and the two independent UAS-*NUAK 548* and UAS-*NUAK 550* insertions were described in Brooks et al., (Brooks et al., 2020). *tn* mutants were described previously (Bawa et al., 2020). The *WT* stock is the w^{1118} strain. Other stocks used were *da*-Gal4 (originally BL37291 outcrossed ten times to w^{1118} to remove background lethal mutations), *pp*l-Gal4 (a gift from L. Dobens), *cg*-Gal4 (BL7011), *mef2*-Gal4 (BL27390), *24B*-Gal4 (BL1767), *c57*-Gal4 (a gift from L. Wallrath), UAS--*lacZ* (BL3956), UAS-*FOXO* (BL9575), UAS-*PTEN* (BL82170), UAS-*InR DN* (BL8252), UAS-*Akt RNAi* (BL31701), UAS-*NUAK RNAi* (BL31885), UAS-*InR CA* (BL8263), UAS-*PTEN RNAi* (BL25841), UAS-*mthl8-3xHA* (FlyORF F002835), UAS-*myc* (BL9675), UAS-*S6K DN* (BL6911), and UAS-*Babo CA* (BL64293). *w; TM3, Sb, e/TM6B, Tb, e* (outcrossed to w^{1118} to analyze *TM6B, Tb*/þ). The *sls-GFP* insertion ($sls^{ZCL2144}$) was kindly provided by Maxim Frolov (Zappia and Frolov, 2016).

2.2. Immunostaining

Wandering L3 larvae were dissected to visualize muscle tissue or individual organs (brain, wing disc, salivary glands, or midgut) and fixed in 4% formaldehyde as described

(Bawa et al., 2020). Primary antibodies used were: rabbit anti-pFOXO (1:200, Abcam), mouse anti-Sls (1:200, Developmental Studies Hybridoma Bank); rabbit anti-CryAB (1:400, BosterBio); mouse anti-Prm (1:200, DSHB), and rabbit anti-Lasp (1:50, a gift from Frieder Schöck) (Fernandes and Schöck, 2014). Fluorescence was detected using the following secondary antibodies: Alexa Flour anti-mouse 488, Alexa Flour anti-rabbit 488, Alexa Flour anti-rat 488, or Alexa Flour anti-mouse 594 (1:400, Molecular Probes, Eugene, OR). F-actin was labeled with phalloidin 405, 488, or 594 (1:400, Molecular Probes, Eugene, OR) and nuclei were stained with Hoechst dye (1:400, Invitrogen, Waltham, MA). Images were captured using a Zeiss 700 confocal microscope. Image processing and analysis was performed using a combination of Zen Black (Zeiss), ImageJ (NIH), and Adobe Photoshop. All images taken at 4x, 10x, or 20x are displayed as maximum intensity projections. Data acquisition at increased magnifications (40x or 63x) are presented as a single plane confocal micrographs.

2.3. Immunoblot analysis

Whole larvae were placed into SDS sample buffer, boiled at 95 °C for 3 min, homogenized, boiled for an additional 10 min at 95 °C, and centrifuged at 20,000×*g* for 1 min to pellet debris. The resulting protein samples were separated by sodium dodecyl sulfate polyacrylamide gel electrophoresis (SDS-PAGE), transferred to polyvinyl difluoride (PVDF) membranes (Pierce Biotechnology, Inc., Waltham, MA), and probed with either rabbit anti-NUAK (1:1000, Genscript), rabbit anti-CryAB (1:1000, BosterBio), rabbit anti-pAkt S505 (1:500, Cell Signaling Technology), rabbit anti-panAkt C67E7 (1:500, Cell Signaling Technology), and mouse anti-ATP5α (1:10000, Abcam, Cambridge, United Kingdom) as a loading control. A peptide-KHL conjugate generated against the C-terminus of NUAK (CRGEYHRIKSKYLDQ) was injected into rabbits and affinity purified by Genscript (Picataway, NJ). Horseradish Peroxidase (HRP) conjugated secondary antibodies (1:5000–1:10000, GE Healthcare, Chicago, IL) were developed using Pierce ECL Plus (Thermo Fisher Scientific) or Prometheus ProSignal Pico detection system (Genesee Scientific, San Diego, CA) and imaged with the FluorChem M system (Protein Simple, San Jose, CA). Quantification of Western blot protein levels was performed using standard densitometric analysis functions in ImageJ.

2.4. RNA sequencing and target gene analysis

RNA sequencing.—Total RNA was collected from 10 muscle carcasses or 3 whole larvae for *mef2>lacZ* control, *mef2>NUAK 548*, or *mef2>NUAK 550* L3 larvae using the RNeasy Mini Kit (Qiagen) and submitted to Genewiz for quality control, library preparation and Illumina HiSeq 2 × 150 bp sequencing. Sequence reads were trimmed to remove adapter sequences and nucleotides with poor quality using Trimmomatic v.0.36. The trimmed reads were mapped to the *Drosophila melanogaster* BDGP6 reference genome available on ENSEMBL using the STAR aligner v.2.5.2b. BAM files were generated as a result of this step. After calculation and extraction of gene hit counts using Subread package v.1.5.2, downstream differential expression analysis was performed with DESeq2. The Wald test was used to generate p-values and log2 fold changes. Genes with an adjusted p-value < 0.05 and absolute log2 fold change >1 were called as differentially expressed genes for each comparison.

Target gene analysis.—Downstream target genes were detected with PathON (https://www.flyrnai.org/tools/pathon/web/) using either muscle as a source tissue and whole larvae or muscle carcass as a target tissue. Comparisons were made using two sets of data, whole larvae or muscle carcass, with *mef2>lacZ* as a control and *mef2>NUAK 548* or *mef2>NUAK 550* as experimental conditions. Confidence was set at high/moderate with a threshold above or below 0.5. Raw and analyzed RNA-Seq data were deposited in the NCBI GEO database under GEO accession GSE204894 (https://www.ncbi.nlm.nih.gov/geo/query/acc.cgi?acc=GSE204894).

2.5. RT-PCR

Relative transcript levels of *mthl8* were assessed in the indicated genotypes using RT-PCR. Total RNA was collected from three wandering L3 larvae in triplicate using the RNeasy Mini Kit (Qiagen). Synthesis of cDNA from 1000 ng RNA was performed using the qScript XLT cDNA SuperMix kit (Quanta Biosciences). For the PCR reactions, RNA was diluted 1:10, Promega GoTaq Flexi buffer and polymerase with the following primers were added:

mthl8 forward 5′-CCGCTGCTCCATGGGAAC, reverse 5′-GCCGCATTTGAGAGATTTGC

rp49 forward 5′-GCCCAAGGGTATCGACAACA, reverse 5′-GCGCTTGTTCGATCCGTAAC;

2.6. Quantification & statistical analysis

Pupal measurements.—Pupa of the appropriate genotype were oriented dorsal side up and attached to slides using a small drop of nail polish. Images were taken on an upright stereomicroscope. Length and width measurements for each pupae were performed in ImageJ using the line and measure functions. Axial ratios (length/width) were calculated in Excel. Raw data of muscles lengths, widths, or axial ratios were imported into Graphpad Prism 6.0 and graphed as a box and whiskers plot. $N \geq 20$ for each genotype.

FOXO nuclear intensity.—Two methods were used to determine the relative distribution of nuclear FOXO. (1) Line plots corresponding to a length of 40 μm measured FOXO intensity across nuclei from single plane confocal images in ImageJ (Analyze > Plot Profile). Raw data values for each genotype (n = 10) were averaged and plotted in GraphPad Prism as an XY line scan. (2) The relative fluorescence intensity of FOXO signal was obtained using the ‘Measure’ function in ImageJ. This mean intensity value was divided by nuclei area and reported as a ratio of *mef2>NUAK 548:mef2>lacZ* signal.

Tissue size measurements.—Z-stack images of each isolated tissue (brain, wing disc, salivary glands, midgut) were used for area measurements. The single plane that contained the maximum area for each organ was fully outlined using the free draw tool followed by the measure command in ImageJ.

Muscle area length measurements.—Z-stack images for each fillet were converted to a maximum intensity projection. The Polylines plugin from ImageJ was used to measure the

length of muscles VL3, VL4, and/or LL1 from dissected L3 individuals. Nuclei area was measured using the circle tool and measure command in ImageJ.

Sarcomere measurements.—For sarcomere number and length measurements in dissected muscle, 20x single plane images were taken of VL3, VL4 and/or LL1 muscles with anti-Sls staining and scale bars were applied using ZEN software. Thick and thin filament lengths were measured in muscle LL1 using anti-Prm or phalloidin from 20x single plane images. For imaging sarcomeres in intact larvae, L3 individuals were heat-killed in 65 °C water and sls-GFP was immediately imaged in muscle DO2 through the cuticle at 20x magnification. In ImageJ, a line was drawn across in focus Z-discs. The length of the line was measured (Analyze → Measure) and a plot of the peak intensities corresponding to Z-discs was generated using the Plot Profile function. The maximum of each peak/Z-disc was found using the BAR plug-in (https://imagej.net/BAR) (BAR → Data Analysis → Find Peaks). The number of sarcomeres/100 μm was determined by dividing the number of maxima by the line length (converted from pixels to microns) × 100. The distance between peaks was calculated from the BAR plot ("List" button on the plot, difference between X1 values after being sorted smallest to largest).

2.7. SUnSET protein synthesis assay

Mef2-Gal4 females were mated with *UAS-lacZ*, *UAS-NUAK RNAi*, *UAS-NUAK 548*, or *UAS-myc* males. The puromycin labeling protocol was adapted from Deliu et al. (Deliu et al., 2017). Eggs were collected for 0–4 h in fresh vials and incubated at 29 °C for 115 h until the L3 stage. Four larvae of each genotype were inverted using a metal probe to expose muscle tissue in Schneider's media and transferred to microcentrifuge tubes containing 1500 μl Schneider's media 5 μg/ml Puromycin (Sigma) on a horizontal shaker at room temperature for 40 min. Larvae were then transferred to a dissection dish for the removal of gut and fat body tissue. Dissected muscle carcasses were transferred to 100 μl 1x protein sample loading buffer (LI-COR Biotechnology), boiled 3 min, homogenized, boiled for another 10 min, and centrifuged at 21130×*g* for 1 min. 10 μl each sample was run on an SDS-PAGE gel. After electro-blotting to nitrocellulose membrane, total protein was visualized with Revert 700 Total Protein Stain (LI-COR Biotechnology) followed by Western blotting with mouse anti-Puromycin 3RH11 (1:1000; Kerafast) and anti-mouse IRDye 680RD antibody (1:10000; (LI-COR Biotechnology). The blot was imaged with the Odyssey XF Imager (LI-COR Biotechnology).

2.8. High sugar diet

High sugar food was made by adding 30% (w/v) of sucrose to standard cornmeal-yeast-agar food (60g sucrose in 200 mL of standard food). Larvae were reared from embryos either on normal or high sugar food. Pupal case and sarcomere measurements were made as described above.

2.9. Feeding assays

Food intake.—L3 larvae were fed on yeast paste plus blue food dye for about 1 h. Larvae were heat killed, rinsed with ddH2O, and then transferred to a slide for imaging.

Mouthhook contractions.—Video recordings for 60 s were taken of wandering L3 larvae on a dish containing apple juice. Mouthhook contractions were manually counted from 30 s of video footage.

Nutrient-rich supplementation.—Larvae were either raised on Molasses Formal food (Genesee Sci Nutri-Fly® MF) or German food (Genesee Sci Nutri-Fly®GF); pupal case measured as described above.

3. Results

3.1. Muscle-specific expression of NUAK reduces pupal and adult body size

We previously showed that loss of NUAK caused muscle degeneration during larval development (Brooks et al., 2020). In a control experiment to demonstrate that muscle-specific expression of NUAK is sufficient to restore *WT* morphology upon loss of NUAK, we induced overexpression (OE) of NUAK alone in muscle tissue using Gal4/UAS-mediated expression (Brand and Perrimon, 1993). Unexpectedly, we observed a reduction in overall pupal size. To substantiate these results, we drove the expression of three independent NUAK OE lines under control of the *mef2* promoter. Compared to *mef2>*þ control pupae, excess NUAK protein expression resulting from a *UAS*-driven *P(EPgy2)* insertion upstream of the *NUAK* transcription start site (*mef2>NUAK EY*), as well as two independent UAS-NUAK insertions (*mef2>NUAK 548* or *mef2>NUAK 550*) all resulted in a small body phenotype when expressed in muscle tissue (Fig. 1A). Expression of *NUAK EY* and *NUAK 548* also produced smaller adults while expression of the *NUAK 550* line was pupal lethal (Fig. 1B). Qualitatively, the increase in phenotype severity upon induction of the *NUAK 550* line suggests that NUAK protein levels may differ among the *NUAK OE* lines. Indeed, Western blot analysis using whole larvae revealed an increase in NUAK protein levels, with *mef>NUAK 550* producing the largest amount of protein (Fig. 1C). Next we tested if the small body size induced by NUAK OE could be phenocopied by expressing NUAK in other tissues. Upregulation of NUAK protein levels by the weak ubiquitous *daughterless (da)*-Gal4 or the fat body *pumpless (ppl)* or *collagen (cg)* Gal4 drivers, exhibited pupal axial ratios (length/width) comparable to *WT* controls. In contrast, we substantiated that *NUAK OE* in muscle tissue caused a smaller pupal size not only with *mef2*-Gal4, but also with *24B*-Gal4 (Fig. 1D).

Feeding deficits were not a primary cause for reduced growth as mouth hook contractions (Fig. S1A) and food ingestion (Fig. S1B) were not compromised in *mef2>NUAK 548* larvae. Moreover, supplementation of larval growth on nutrient-rich media (*i.e.,* German food) did not alter the final size of pupae overexpressing NUAK compared to those reared on a standard molasses, cornmeal diet (Fig. S1C). As a positive control, the growth phenotype of *thin (tn)* mutants was partially suppressed when grown on German food, consistent with our previously published data that amino acids provide building blocks for muscle growth (Bawa et al., 2020). These data demonstrate that muscle-specific expression of NUAK influences organismal size during development and compromises the ability of adults to achieve a physiologically normal body size independent of nutritional status.

3.2. NUAK OE phenocopies loss of insulin signaling

To determine how *mef2*-mediated expression of NUAK affects organismal size, we performed RNAseq analysis on either whole larvae or muscle carcass using two independent NUAK transgenes (*UAS-NUAK 548* and *UAS-NUAK 550*) that showed markedly elevated levels of NUAK protein (Fig. 1C). Differential gene expression (DEG) analysis between control *mef2>lacZ* vs. *mef2>NUAK* larvae revealed a similar number of significantly regulated genes in muscle fillets, while the total number of genes identified in whole larvae was much higher in *mef2>NUAK 550* samples (Fig. 2A). Despite a difference in the total number of DEGs identified upon OE of *NUAK 548* or *NUAK 550*, the relative percentage of up- or down-regulated genes was comparable in whole larvae, but increased for up-regulated genes in *NUAK 550* muscle carcass (Fig. 2B).

The striking reduction in pupal and adult body size upon muscle-specific NUAK OE implies signals emanating from muscle tissue regulate organismal size. To determine which signaling pathways(s) may be responsible for this intertissue communication, we utilized PathON (https://www.flyrnai.org/tools/pathon/web/), a pathway analysis tool designed for *Drosophila* RNA seq datasets. Using muscle as a 'source' tissue and whole larvae as the 'target' or receiving tissue, we looked for enrichment of signaling pathways typically associated with the control of body size. Indeed, pathway target genes downstream of insulin signaling were prominent in both *NUAK 548* and *NUAK* 550 RNA seq datasets, especially compared to the low number of target genes linked to the TGFβ pathway (Fig. 2C).

Next we assessed the identity of individual gene targets that were either up- or down-regulated in *mef2>NUAK 548* and *mef2>NUAK 550* whole larvae or muscle carcasses. Out of the 47 or 48 total genes that were common in whole larvae or muscle carcass datasets, respectively, six genes appeared in both (Fig. 2D, bold font). Two genes that showed lower levels of gene expression were *CG12224*, a putative dehydrogenase, and *Outer segment 5 (Oseg5)*, a gene that encodes for a WD40 repeat-containing protein required for cilium assembly (Avidor-Reiss et al., 2004). In addition to the 3–5-fold up-regulation of *NUAK* (Fig. 2E), other genes that showed similar levels of increased expression were *lethal (2) essential for life [l(2)efl]* and *Gamma-interferon-inducible lysosomal thiol reductase 3 (GILT3)*. *l(2)efl* encodes for the small heat shock protein CryAB, which is a known target of FOXO signaling in other tissues (Flatt et al., 2008). We validated increased protein levels of CryAB upon OE of both *FOXO* and *NUAK 548* (Fig. 2F). Two other upregulated insulin pathway targets, *CG32698* and *Thor* (Jünger et al., 2003; Puig et al., 2003; Teleman et al., 2008; Wang et al., 2005), were present in either the whole larvae (*CG32698*) or muscle carcass (*Thor*) datasets (Fig. 2E). A novel target with 7 to 10-fold increased expression in both whole larvae and muscle carcass was *methuselah-like 8 (mthl8)*, a predicted G protein-coupled receptor possibly linked to aging or stress responses (de Mendoza et al., 2016). To determine if *mthl8* is also an insulin pathway target, we performed RT-PCR. Both *mef2>NUAK 548* and *mef>FOXO* showed higher levels of *mthl8* transcript, which was not detectable in control larvae (*mef2>lacZ*) (Fig. 2G). In addition to *CryAB, CG32698*, and *Thor*, we have identified *mthl8* as a new, common target of both NUAK and insulin signaling.

Multiple outputs of insulin signaling were examined to determine a link between NUAK and the insulin pathway. As a measure of organismal growth, we first assessed pupal size using the *mef2*-Gal4 driver to induce muscle expression of the indicated *UAS*-transgenes. Quantitation confirmed a decrease in pupal case lengths upon *NUAK OE* (Fig. 3A). Expression of either *FOXO* or *PTEN*, both negative regulators of the insulin pathway, also caused reduced organismal growth, consistent with previous observations (Demontis and Perrimon, 2009). Muscle expression of *mthl8* also negatively impacted pupal length (Fig. 3A), possibly highlighting a role for *mthl8* in the regulation of body size. Moreover, this reduction in body size by *mthl8 OE* was suppressed upon removal of a single copy of *NUAK*, demonstrating a genetic interaction between these two genes that together impinge on organismal size (Fig. S2A).

Two pieces of evidence show that insulin signaling is altered upon muscle-specific NUAK expression. First, we observed a loss of phospho-Akt (pAkt) by Western blotting. The decrease in pAkt signal was slight in *mef2>NUAK 548* larvae, but nearly complete in *mef2>NUAK 550* larvae, especially when compared to the low levels of pAkt after induction of a dominant-negative insulin receptor (*mef2>InR DN*) (Fig. 3B). Since these experiments were performed in whole larvae, we next assessed insulin signaling at the tissue level by examining the subcellular localization of FOXO. FOXO is phosphorylated and inactive in the cytoplasm, while nuclear FOXO protein is capable of altering gene expression in response to oxidative stress and other insults to limit growth when nutrients are scarce (Jünger et al., 2003; Puig et al., 2003). *Mef2*-induced muscle expression of NUAK resulted in the nuclear translocation of FOXO compared to *mef2>lacZ* muscles alone as depicted by representative images and line plot analyses across multiple nuclei (Fig. 3C). The relative intensity of FOXO accumulation (mean intensity/nuclei area) was approximately 3.5x in *mef>NUAK 548* nuclei compared to *mef2>lacZ* controls. These data, combined with validation of FOXO-specific transcriptional targets upon NUAK OE, are consistent with reduced insulin signaling in muscle tissue.

Deficits in insulin signaling cause a reduction in both non-endoreplicating (brain and wing disc) and endoreplicating (salivary gland and midgut) tissues (Demontis and Perrimon, 2009), while loss of the Actβ→TGFβ pathway reduces the size of a subset of polyploid tissues with no effect on brain or wing disc growth (Moss-Taylor et al., 2019). Consistent with our RNA seq results whereby insulin pathway targets are preferentially changed over TGFβ pathway targets, we also observed a general reduction in the size of each organ measured. All three *mef2>NUAK OE* lines showed a trend of decreased tissue size, with the strongest *NUAK 550* transgene exhibiting the most pronounced effect (Fig. 3D). These results are similar to qualitative observations whereby multiple tissues are smaller upon muscle-specific overexpression of PTEN (Demontis and Perrimon, 2009). To confirm these prior observations, we measured the size of individual organs in *mef2>FOXO* and *mef2>PTEN* animals and although variable, the overall trend showed a reduction of tissue size at the organ level (Fig. 3E).

Since induction of NUAK expression in the larval body wall muscles reduces overall organismal growth, we predicted that the area of this particular polyploid tissue would also be smaller. Indeed, low magnification images of carcass fillets revealed an overall reduction

in muscle size compared to *mef2*-Gal4 controls (Fig. S3A). Measurements confirmed a consistent reduction in the area of the ventral longitudinal 3 (VL3), ventral longitudinal 4 (VL4) (Fig. 4A and B), and lateral longitudinal 1 (LL1) (Figs. S3A–C) muscles that correlate with increased NUAK protein expression (Fig. 1C). We also observed an increase in aberrant muscle morphology towards the visceral side of muscles with increasing NUAK expression, although the implications of this are not yet clear (Fig. S3B). One additional feature of reduced insulin signaling that was recapitulated in *NUAK OE* muscles was a decrease in the area of each nuclei (Fig. 4C). Surprisingly, there were also more nuclei (Fig. S3D), suggesting an increase in embryonic myoblast fusion.

Analysis of muscle area (Fig. 4B; Fig. S3C) upon a block in insulin signaling (*mef2>FOXO* or *mef2>PTEN*) showed a reduction similar to that of *NUAK OE*, more closely resembling the *NUAK 550* line. Even though muscle lengths in all genotypes were decreased, muscle width measurements were more severely affected upon *FOXO* or *PTEN OE* (Figs. S3E and F), supporting published data that different signals control longitudinal vs girth muscle growth (Kim and O'Connor, 2021). A link between NUAK and insulin signaling is further supported by genetic interaction data, whereby loss of a single copy of *NUAK* partially suppresses the reduction in pupal and muscle length caused by excess insulin signaling (Figs. S4A and B). These results, taken together, support a non-autonomous role for NUAK, similar to that of insulin, in the regulation of tissue and body size.

3.3. Sarcomere remodeling

While analyzing muscle area, we observed that the overall width of striations labeled with phalloidin within the smaller *NUAK OE* muscles appeared broader than in *mef2>lacZ* controls (compare yellow line in all panels in Fig. 4A). Since phalloidin labels F-actin that comprises the thin filament attached to each Z-disc, these observations suggested fewer sarcomeres along the length of the muscle. Using an antibody directed against the Z-disc as a proxy for sarcomere number, we counted the number of sarcomeres within a defined distance (100 μm). Analysis of sarcomere number/100 μm in various genotypes fell into three distinct classes (Fig. 5A and B). Class I, or *mef2>lacZ* control muscles, contained approximately 12–15 sarcomeres/100 μm. Sarcomeres designated as Class II showed a remarkably consistent reduction in the relative number of sarcomeres and was prevalent among *NUAK OE* or in genotypes that reduced insulin signaling (*mef2>FOXO* or *mef2>PTEN*). Conversely, enhanced insulin pathway activity via expression of a constitutively-active insulin receptor (InR CA) or knockdown of the negative regulator *PTEN*, as well as *NUAK RNAi*, all increased the number of sarcomeres/100 μm beyond that of control muscles (Class III). Measurements of sarcomere length proved to be inversely proportional to sarcomere number/100 μm. *NUAK OE* or insulin loss caused wider sarcomeres, while insulin activation resulted in shorter sarcomeres (Fig. 5C). Comparable results were obtained with *mef2>NUAK OE* imaging and quantitation of sls-GFP through the cuticle in intact L3 larvae, confirming that manual dissection of larval muscles did not alter sarcomere parameters (Figs. S5A–C).

To determine if the observed sarcomere alterations are a conserved feature of smaller muscles, we assessed the relative sarcomere number and sarcomere length in additional

genotypes. Muscle expression of *mthl8* (*mef2>mthl8_HA*) or mutations in *Tubby (Tb)* (Guan et al., 2006; Lindsley, 1973) both showed diminished body size (Fig. 3A) and shorter muscles (Fig. S3E), but did not exhibit the same trend in sarcomere number/100 μm (Fig. 5B) or sarcomere length increase (Fig. 5C) observed in Class II mutants. Appreciable differences in sarcomere parameters were only observed in *mef2>NUAK EY + mthl8_HA* muscles compared to *mef2>NUAK EY + lacZ* or *mef2>mthl8_HA* alone (Figs. S2B and C) where significant enhancement of phenotypes was observed. For *Tb* mutants, the number of sarcomeres was increased even to a greater extent than activated insulin signaling, further demonstrating that muscle size and sarcomere alterations can be uncoupled.

While *mef2* promoter activity is predominant in myocytes and highly expressed throughout muscle development, it also regulates gene expression in subsets of neurons (Blanchard et al., 2010). To confirm that the sarcomere remodeling effects are intrinsic to muscle tissue, we utilized the larval body wall muscle driver *C57*-Gal4 (Dialynas et al., 2010; Koh et al., 1999). The reduction in pupal size or muscle length was similar using either the *mef2* or *C57*-Gal4 lines to regulate *NUAK 548* expression (Fig. 5D). Moreover, the reduction in relative sarcomere number and increase in sarcomere width under control of *C57* mirrored the results obtained with *mef2*-Gal4 (Fig. 5E, compare to Fig. 5B and C). Collectively, these results show that NUAK and insulin signaling have the capacity to actively adjust the amount and/or size of sarcomeres throughout muscle growth.

To further understand how modulation of NUAK and FOXO affects sarcomere size, we next assessed the relative length of the thin and thick filaments in each genotype. F-actin is attached to the Z-disc and extends in opposite directions to comprise the thin filament, while Paramyosin (Prm) is a component of the thick filament. Measurements of both thin filament and thick filament length (Fig. 6A and B), assessed by phalloidin and Prm labeling, respectively, were remarkably similar within Class II and Class III genotypes, indicating that both major structural features of the contractile apparatus are appropriately scaled together in response to altered intracellular signaling.

3.4. Aberrant insulin signaling alters sarcomeric Lasp localization

Since *Drosophila* Lasp protein has been shown to regulate thin filament length and the relative spacing between filaments (Fernandes and Schöck, 2014), we next chose to examine the distribution of Lasp in muscles that exhibit variations in sarcomere size. In control *mef2>lacZ* muscles, Lasp was prominent at the Z-disc and the A-band where thick and thin filaments overlap (Fig. 7A) (Fernandes and Schöck, 2014). This distinct Z-disc localization was lost in muscles expressing *NUAK EY* or *NUAK 548* and instead became punctate in regions surrounding the Z-disc. Moreover, the A band localization of Lasp disappeared, possibly accounting for the wider thin filament bands denoted by phalloidin staining. Similarly, *FOXO OE* or *PTEN OE* showed diffuse Lasp localization and wider F-actin patterning. RNAi knockdown of *NUAK*, *mtlh8 OE*, and *Tb* mutants all retained relatively normal Lasp distribution.

Since activation of insulin signaling increases the relative sarcomere number during larval muscle growth, we hypothesized that loss of NUAK could promote general protein translation. Indeed, RNA seq analysis of *NUAK −/−* vs *WT* whole larvae revealed an

upregulation of transcripts that promote eukaryotic translation initiation (Fig. S6A). While incorporation of puromycin into newly synthesized proteins using the SUnSET method was increased upon Myc overexpression as previously reported (Deliu et al., 2017), neither *NUAK* mutants nor *NUAK OE* muscles showed any difference in global protein translation compared to *WT* individuals (Fig. S6B). However, we were able to detect a decrease in Lasp protein levels in muscles with excess *NUAK* expression (Fig. S6C). These data suggest that while global protein translation is not altered, the relative protein levels and/or sarcomere localization of specific muscle proteins, such as Lasp, are subject to regulation by NUAK and by extension, the insulin pathway.

4. Discussion

In this study, we have found that induction of NUAK in muscle tissue blocks insulin signaling and compromises growth to produce smaller pupae and adults. Accordingly, this overall reduction in growth limits the size of both non-endoreplicating and endoreplicating larval tissues, including muscles. However, we were surprised to discover that reduced muscle and organismal size can be uncoupled from alterations in sarcomere number or size, suggesting that independent mechanisms control this muscle-intrinsic process of sarcomere remodeling.

4.1. Mthl8 as a novel regulator of systemic growth

The Methuselah-type family of G-protein-coupled receptors (GPCRs) form the B3 subgroup of GPCRs and are characterized by an extended N-terminal ectodomain, a seven transmembrane domain, and a short intracellular C-terminal domain (de Mendoza et al., 2016). While the functional role of the majority of the 16 mthl gene products is unknown, mutations in the founding member *methuselah (mth)* exhibit extended lifespan and resistance to various stresses, including starvation (Lin et al., 1998). Methuselah-like 1 (Mthl1) is a receptor for the secreted ligand Folded gastrulation (Fog) that promotes epithelial morphogenetic shape changes during embryonic gastrulation (Manning et al., 2013). In *Tribolium*, the *mthl* genes have different developmental expression patterns and all enhance resistance to starvation in addition to having effects on development, lifespan, and reproduction (Li et al., 2014). More recent reports have shown that Mtl is required in insulin-producing cells (IPCs) (Gimenez et al., 2013) and can modulate physiological insulin levels in response to nutrients (Delanoue and Léopold, 2013). Thus, it seems reasonable to propose that Mthl8 functions in muscle tissue to modulate either a tissue-specific or systemic response to insulin signaling. Further experiments will be needed to identify the ligand that regulates Mthl8 activity and to determine how it impacts insulin signal transduction.

The TGFβ ligands Myostatin and Activin negatively regulate mammalian skeletal muscle size (Kollias and McDermott, 2008). However, a different mechanism operates in *Drosophila*, whereby inactivation of *Drosophila* Actβ causes smaller body size, including reduced muscle area (Moss-Taylor et al., 2019). Relevant to this study, the O'Connor lab further demonstrated that Actβ signaling positively regulates muscle mass through the addition of new sarcomere components to increase muscle length and width (Kim and

O'Connor, 2021). Interestingly, serial sarcomere addition is dependent on Actβ signaling as mutations in genes encoding for Actβ, the Baboon (Babo) receptor, or the Smad2 transcription factor all reduce sarcomere addition. Consistent with their results, we also observed an increase in sarcomere number/100 μm upon expression of a constitutively active (CA) Babo receptor (*mef2>Babo CA)* (Fig. S7). The O'Connor lab also reported that muscle expression of *Pdk RNAi*, *S6K RNAi* or *S6K CA* did not alter Z-disc addition. In our hands, testing additional components that either activate (*InR CA, PTEN RNAi*) or inhibit (*FOXO OE, PTEN OE, Akt RNAi*) insulin pathway activity, we indeed see a clear effect on sarcomere remodeling, but not upon expression of *S6K DN (*Fig. S7). One likely explanation is that blocking insulin via NUAK OE or upon manipulating insulin pathway components routes signal transduction through FOXO, but not the S6K branch, thus limiting new protein synthesis and sarcomere addition.

4.2. Independent control of muscle size and sarcomere alterations

The number of sarcomeres in series along the length of a muscle may vary among different muscles, but each individual sarcomere largely exhibits a standard force-length relationship (Gordon et al., 1966; Lieber et al., 2017; Rassier, 2017). For muscles within a given species, optimal overlap between thick and thin filaments generates maximal force (Burkholder and Lieber, 2001). For longer sarcomeres, a decrease in the number of actin-myosin interactions reduces force. This simple length-tension association assumes that each sarcomere follows an individual force-length relationship and does not take into account complexities of sarcomere nonuniformity across muscles (Johnston et al., 2016; Rassier, 2017). Thick filament lengths are remarkably consistent across different vertebrate muscles, while thin filament lengths are highly variable across muscle types and organisms (Castillo et al., 2009; Gokhin et al., 2012; Granzier et al., 1991; Ringkob et al., 2004). Accordingly, due to aging or disease after initial myofibril assembly, this remodeling of thin filament components could result from differences in thick (MHC isoform expression) or thin (tropomyosin and/or troponin) filament protein expression, as well as post-translational modifications or proteolysis that influences thin filament dynamics (Gokhin et al., 2014; Gokhin and Fowler, 2013).

In *Drosophila* larval muscles, the lengths of both thin and thick filaments scale accordingly, whereby genotypes with wider or thinner sarcomeres show an increase or decrease in the length of both thin and thick filaments, respectively. Even in myofibers with wider, but fewer sarcomeres, overall muscle force is not expected to change since the relative overlap between actin and myosin molecules are proportionally maintained. Conversely, muscles with shorter sarcomeres compensate for reduced force within each sarcomere unit through the serial addition of new sarcomeres. Intriguingly, this ability to remodel sarcomeres is not a general feature of smaller muscles due to decreased organismal growth. Both pupal case and muscle size are reduced upon *mthl8 OE* or in *Tb* mutants, yet there is an inverse correlation of sarcomere number and length compared to muscles with reduced insulin signaling. Moreover, this sarcomere plasticity is independent of insulin resistance as larvae fed on a high sugar diet exhibited reduced organismal growth (Musselman et al., 2011), yet showed a trend similar to *Tb* mutants, with greater sarcomere numbers and reduced

length (Figs. S8A and B). Thus, larval muscles must possess sensing mechanisms that affect muscle-intrinsic sarcomere remodeling.

4.3. Intracellular targets of NUAK kinase activity

What is/are the substrate(s) of NUAK kinase activity that limit growth and/or promotes sarcomere remodeling? Human NUAK1 is highly expressed in mouse soleus muscle, an oxidative tissue that exhibits enhanced insulin-stimulated glucose transport over glycolytic muscles (Inazuka et al., 2012). Inazuka et al. provide evidence that NUAK1 regulates glucose metabolism in skeletal muscle through negative regulation of the insulin pathway. Phosphoproteome analysis of NUAK1-deficient muscle tissue revealed a decrease in the phosphorylation of Insulin-receptor substrate (IRS-1) at Ser-1097, a modification known to block tyrosine phosphorylation (Tyr-608) and prevent insulin signaling. A concomitant increase in the phosphorylation of Tyr-608 and Akt confirmed activation of insulin signaling and glucose uptake upon loss of NUAK. Thus, it is possible that *Drosophila* NUAK acts in a similar fashion to mediate negative feedback of insulin activity via phosphorylation of Chico/IRS-1 to prevent insulin-mediated glucose metabolism to limit larval muscle growth. Phosphorylation of the sarcomere proteins Myosin and Titin were also decreased upon muscle-specific knockout of NUAK1, consistent with observations that the *C. elegans* ortholog Unc-82 may phosphorylate Myosin and Paramyosin (Hoppe et al., 2010; Schiller et al., 2017).

5. Conclusions

Two important conclusions emerge from our results regarding NUAK or insulin signaling in muscle tissue. First, there must be an intrinsic mechanism to precisely control sarcomere number and spacing despite differences in total muscle length. Second, the inverse relationship between sarcomere number and length suggests that the muscle is able to sense sarcomere number and modulate length accordingly. Future experiments will focus on understanding the interplay between muscle growth and sarcomere remodeling in response to altered signaling within and between tissues during development.

Supplementary Material

Refer to Web version on PubMed Central for supplementary material.

Acknowledgements

We would first like to thank Lori Wallrath, Mary Baylies, and Fabio DeMontis for helpful discussion and suggestions, as well as the contributions of Xena Moore, Adrienne Alder, and Everett Montalvo for technical assistance. We greatly appreciate the anti-Lasp antisera from Frieder Schöck. Stocks obtained from the Bloomington *Drosophila* Stock Center (NIH P40OD018537) and Zurich ORFeome Project were used in this study (Bischof et al., 2013). The graphical abstract and panel 3F in Supplemental Fig. 3 were created in Biorender.com.

Funding

This study was supported by the National Institute of Arthritis and Musculoskeletal and Skin Diseases (NIAMS) of the National Institutes of Health (NIH) under award number RO1AR060788 and the Supplements to Advance Research (STAR) program, both awarded to E.R.G.

References

Avidor-Reiss T, Maer AM, Koundakjian E, Polyanovsky A, Keil T, Subramaniam S, Zuker CS, 2004. Decoding cilia function: defining specialized genes required for compartmentalized cilia biogenesis. Cell 117, 527–539. [PubMed: 15137945]

Bawa S, Brooks DS, Neville KE, Tipping M, Sagar MA, Kollhoff JA, Chawla G, Geisbrecht BV, Tennessen JM, Eliceiri KW, Geisbrecht ER, 2020. TRIM32 cooperates with glycolytic enzymes to promote cell growth. Elife 9.

Beadle G, Tatum E, Clancy C, 1938. Food level in relation to rate of development and eye pigmentation in Drosophila melanogaster. Biol. Bull 447–462.

Biglou SG, Bendena WG, Chin-Sang I, 2021. An overview of the insulin signaling pathway in model organisms Drosophila melanogaster and Caenorhabditis elegans. Peptides 145, 170640. [PubMed: 34450203]

Bischof J, Björklund M, Furger E, Schertel C, Taipale J, Basler K, 2013. A versatile platform for creating a comprehensive UAS-ORFeome library in Drosophila. Development 140, 2434–2442. [PubMed: 23637332]

Blanchard FJ, Collins B, Cyran SA, Hancock DH, Taylor MV, Blau J, 2010. The transcription factor Mef2 is required for normal circadian behavior in Drosophila. J. Neurosci 30, 5855–5865. [PubMed: 20427646]

Brand AH, Perrimon N, 1993. Targeted gene expression as a means of altering cell fates and generating dominant phenotypes. Development 118, 401–415. [PubMed: 8223268]

Brooks D, Naeem F, Stetsiv M, Goetting SC, Bawa S, Green N, Clark C, Bashirullah A, Geisbrecht ER, 2020. Drosophila NUAK functions with Starvin/BAG3 in autophagic protein turnover. PLoS Genet. 16, e1008700. [PubMed: 32320396]

Burkholder TJ, Lieber RL, 2001. Sarcomere length operating range of vertebrate muscles during movement. J. Exp. Biol 204, 1529–1536. [PubMed: 11296141]

Castillo A, Nowak R, Littlefield KP, Fowler VM, Littlefield RS, 2009. A nebulin ruler does not dictate thin filament lengths. Biophys. J 96, 1856–1865. [PubMed: 19254544]

de Mendoza A, Jones JW, Friedrich M, 2016. Methuselah/Methuselah-like G protein-coupled receptors constitute an ancient metazoan gene family. Sci. Rep 6, 21801. [PubMed: 26915348]

Delanoue R, Léopold P, 2013. Developmental biology: miRs and steroids and growth control. Curr. Biol 23, R328–R330. [PubMed: 23618672]

Deliu LP, Ghosh A, Grewal SS, 2017. Investigation of protein synthesis in Drosophila larvae using puromycin labeling. Biol Open 6, 1229–1234. [PubMed: 28642244]

Demontis F, Perrimon N, 2009. Integration of Insulin receptor/Foxo signaling and dMyc activity during muscle growth regulates body size in Drosophila. Development 136, 983–993. [PubMed: 19211682]

Dialynas G, Speese S, Budnik V, Geyer PK, Wallrath LL, 2010. The role of Drosophila Lamin C in muscle function and gene expression. Development 137, 3067–3077. [PubMed: 20702563]

Droujinine IA, Perrimon N, 2016. Interorgan communication pathways in physiology: focus on Drosophila. Annu. Rev. Genet 50, 539–570. [PubMed: 27732790]

Fernandes I, Schöck F, 2014. The nebulin repeat protein Lasp regulates I-band architecture and filament spacing in myofibrils. J. Cell Biol 206, 559–572. [PubMed: 25113030]

Flatt T, Min KJ, D'Alterio C, Villa-Cuesta E, Cumbers J, Lehmann R, Jones DL, Tatar M, 2008. Drosophila germ-line modulation of insulin signaling and lifespan. Proc. Natl. Acad. Sci. U. S. A 105, 6368–6373. [PubMed: 18434551]

Garofalo RS, 2002. Genetic analysis of insulin signaling in Drosophila. Trends Endocrinol. Metabol 13, 156–162.

Gautel M, Djinović-Carugo K, 2016. The sarcomeric cytoskeleton: from molecules to motion. J. Exp. Biol 219, 135–145. [PubMed: 26792323]

Gimenez LE, Ghildyal P, Fischer KE, Hu H, Ja WW, Eaton BA, Wu Y, Austad SN, Ranjan R, 2013. Modulation of methuselah expression targeted to Drosophila insulin-producing cells extends life and enhances oxidative stress resistance. Aging Cell 12, 121–129. [PubMed: 23121290]

Gokhin DS, Dubuc EA, Lian KQ, Peters LL, Fowler VM, 2014. Alterations in thin filament length during postnatal skeletal muscle development and aging in mice. Front. Physiol 5, 375. [PubMed: 25324783]

Gokhin DS, Fowler VM, 2013. A two-segment model for thin filament architecture in skeletal muscle. Nat. Rev. Mol. Cell Biol 14, 113–119. [PubMed: 23299957]

Gokhin DS, Kim NE, Lewis SA, Hoenecke HR, D'Lima DD, Fowler VM, 2012. Thin-filament length correlates with fiber type in human skeletal muscle. Am. J. Physiol. Cell Physiol 302, C555–C565. [PubMed: 22075691]

Gordon AM, Huxley AF, Julian FJ, 1966. The variation in isometric tension with sarcomere length in vertebrate muscle fibres. J. Physiol 184, 170–192. [PubMed: 5921536]

Granzier HL, Akster HA, Ter Keurs HE, 1991. Effect of thin filament length on the force-sarcomere length relation of skeletal muscle. Am. J. Physiol 260, C1060–C1070. [PubMed: 2035614]

Guan X, Middlebrooks BW, Alexander S, Wasserman SA, 2006. Mutation of TweedleD, a member of an unconventional cuticle protein family, alters body shape in Drosophila. Proc. Natl. Acad. Sci. U. S. A 103, 16794–16799. [PubMed: 17075064]

Hoppe PE, Chau J, Flanagan KA, Reedy AR, Schriefer LA, 2010. Caenorhabditis elegans unc-82 encodes a serine/threonine kinase important for myosin filament organization in muscle during growth. Genetics 184, 79–90. [PubMed: 19901071]

Hu X, Cherbas L, Cherbas P, 2003. Transcription activation by the ecdysone receptor (EcR/USP): identification of activation functions. Mol. Endocrinol 17, 716–731. [PubMed: 12554759]

Inazuka F, Sugiyama N, Tomita M, Abe T, Shioi G, Esumi H, 2012. Muscle-specific knock-out of NUAK family SNF1-like kinase 1 (NUAK1) prevents high fat diet-induced glucose intolerance. J. Biol. Chem 287, 16379–16389. [PubMed: 22418434]

Johnston K, Jinha A, Herzog W, 2016. The role of sarcomere length non-uniformities in residual force enhancement of skeletal muscle myofibrils. R. Soc. Open Sci 3, 150657. [PubMed: 27069655]

Jorgenson KW, Phillips SM, Hornberger TA, 2020. Identifying the structural adaptations that drive the mechanical load-induced growth of skeletal muscle: a scoping review. Cells 9 (7), 1658.

Jünger MA, Rintelen F, Stocker H, Wasserman JD, Végh M, Radimerski T, Greenberg ME, Hafen E, 2003. The Drosophila forkhead transcription factor FOXO mediates the reduction in cell number associated with reduced insulin signaling. J. Biol 2, 20. [PubMed: 12908874]

Kim MJ, O'Connor MB, 2021. Activin signaling promotes muscle growth through InR/TORC1-dependent and -independent processes. Development vol. 148.

Koh YH, Popova E, Thomas U, Griffith LC, Budnik V, 1999. Regulation of DLG localization at synapses by CaMKII-dependent phosphorylation. Cell 98, 353–363. [PubMed: 10458610]

Kollias HD, McDermott JC, 2008. Transforming growth factor-beta and myostatin signaling in skeletal muscle. J. Appl. Physiol 104, 579–587, 1985. [PubMed: 18032576]

Koyama T, Mendes CC, Mirth CK, 2013. Mechanisms regulating nutrition-dependent developmental plasticity through organ-specific effects in insects. Front. Physiol 4, 263. [PubMed: 24133450]

Koyama T, Texada MJ, Halberg KA, Rewitz K, 2020. Metabolism and growth adaptation to environmental conditions in Drosophila. Cell. Mol. Life Sci 77, 4523–4551. [PubMed: 32448994]

Kramer JM, Davidge JT, Lockyer JM, Staveley BE, 2003. Expression of Drosophila FOXO regulates growth and can phenocopy starvation. BMC Dev. Biol 3, 5. [PubMed: 12844367]

Li C, Zhang Y, Yun X, Wang Y, Sang M, Liu X, Hu X, Li B, 2014. Methuselah-like genes affect development, stress resistance, lifespan and reproduction in Tribolium castaneum. Insect Mol. Biol 23, 587–597. [PubMed: 24924269]

Lieber RL, Roberts TJ, Blemker SS, Lee SSM, Herzog W, 2017. Skeletal muscle mechanics, energetics and plasticity. J. NeuroEng. Rehabil 14, 108. [PubMed: 29058612]

Lin YJ, Seroude L, Benzer S, 1998. Extended life-span and stress resistance in the Drosophila mutant methuselah. Science 282, 943–946. [PubMed: 9794765]

Lindsley D, 1973. Drosophila Inf Serv, p. 21.

Manning AJ, Peters KA, Peifer M, Rogers SL, 2013. Regulation of epithelial morphogenesis by the G protein-coupled receptor mist and its ligand fog. Sci. Signal 6, ra98. [PubMed: 24222713]

Mirth C, Truman JW, Riddiford LM, 2005. The role of the prothoracic gland in determining critical weight for metamorphosis in Drosophila melanogaster. Curr. Biol 15, 1796–1807. [PubMed: 16182527]

Mirth CK, Shingleton AW, 2012. Integrating body and organ size in Drosophila: recent advances and outstanding problems. Front. Endocrinol 3, 49.

Moss-Taylor L, Upadhyay A, Pan X, Kim MJ, O'Connor MB, 2019. Body size and tissue-scaling is regulated by motoneuron-derived activinß in. Genetics 213, 1447–1464. [PubMed: 31585954]

Musselman LP, Fink JL, Narzinski K, Ramachandran PV, Hathiramani SS, Cagan RL, Baranski TJ, 2011. A high-sugar diet produces obesity and insulin resistance in wild-type Drosophila. Dis. Model Mech 4, 842–849. [PubMed: 21719444]

Nässel DR, Liu Y, Luo J, 2015. Insulin/IGF signaling and its regulation in Drosophila. Gen. Comp. Endocrinol 221, 255–266. [PubMed: 25616197]

Puig O, Marr MT, Ruhf ML, Tjian R, 2003. Control of cell number by Drosophila FOXO: downstream and feedback regulation of the insulin receptor pathway. Genes Dev. 17, 2006–2020. [PubMed: 12893776]

Rassier DE, 2017. Sarcomere mechanics in striated muscles: from molecules to sarcomeres to cells. Am. J. Physiol. Cell Physiol 313, C134–C145. [PubMed: 28539306]

Ringkob TP, Swartz DR, Greaser ML, 2004. Light microscopy and image analysis of thin filament lengths utilizing dual probes on beef, chicken, and rabbit myofibrils. J. Anim. Sci 82, 1445–1453. [PubMed: 15144085]

Schiller NR, Duchesneau CD, Lane LS, Reedy AR, Manzon ER, Hoppe PE, 2017. The role of the UNC-82 protein kinase in organizing myosin filaments in striated muscle of. Genetics 205, 1195–1213. [PubMed: 28040740]

Schwedes CC, Carney GE, 2012. Ecdysone signaling in adult Drosophila melanogaster. J. Insect Physiol 58, 293–302. [PubMed: 22310011]

Shingleton AW, Das J, Vinicius L, Stern DL, 2005. The temporal requirements for insulin signaling during development in Drosophila. PLoS Biol. 3, e289. [PubMed: 16086608]

Stieper BC, Kupershtok M, Driscoll MV, Shingleton AW, 2008. Imaginal discs regulate developmental timing in Drosophila melanogaster. Dev. Biol 321, 18–26. [PubMed: 18632097]

Takano K, Watanabe-Takano H, Suetsugu S, Kurita S, Tsujita K, Kimura S, Karatsu T, Takenawa T, Endo T, 2010. Nebulin and N-WASP cooperate to cause IGF-1-induced sarcomeric actin filament formation. Science 330, 1536–1540. [PubMed: 21148390]

Teleman AA, Hietakangas V, Sayadian AC, Cohen SM, 2008. Nutritional control of protein biosynthetic capacity by insulin via Myc in Drosophila. Cell Metabol. 7, 21–32.

Texada MJ, Koyama T, Rewitz K, 2020. Regulation of body size and growth control. Genetics 216, 269–313. [PubMed: 33023929]

Wang MC, Bohmann D, Jasper H, 2005. JNK extends life span and limits growth by antagonizing cellular and organism-wide responses to insulin signaling. Cell 121, 115–125. [PubMed: 15820683]

Yao TP, Segraves WA, Oro AE, McKeown M, Evans RM, 1992. Drosophila ultraspiracle modulates ecdysone receptor function via heterodimer formation. Cell 71, 63–72. [PubMed: 1327536]

Zappia MP, Frolov MV, 2016. E2F function in muscle growth is necessary and sufficient for viability in Drosophila. Nat. Commun 7, 10509. [PubMed: 26823289]

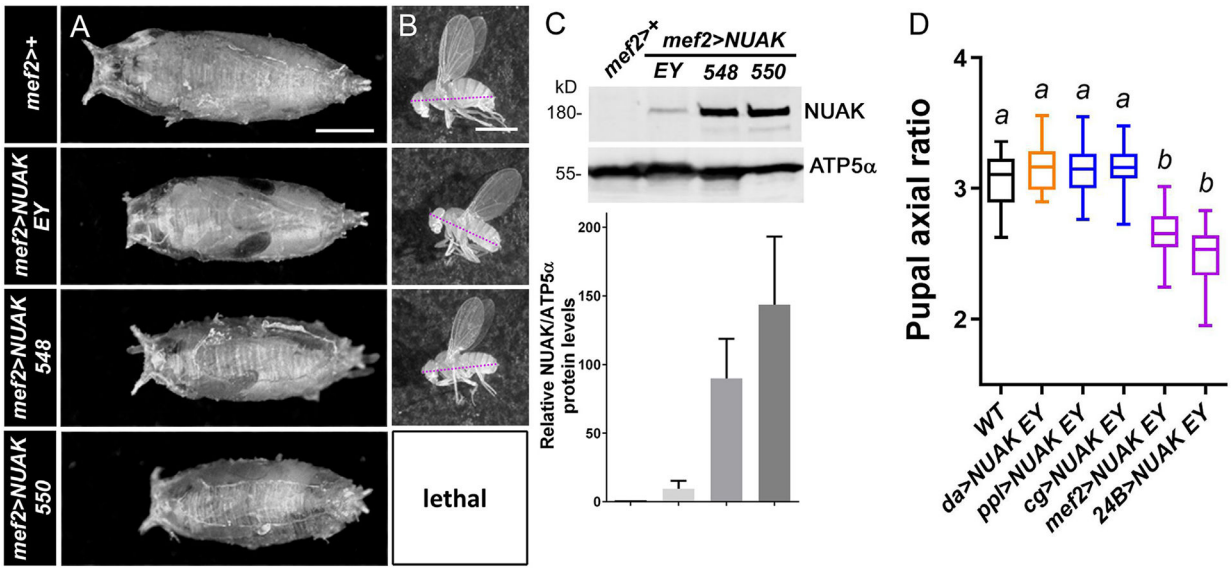

Fig. 1. Increasing levels of NUAK in muscle tissue limits organismal size.

(A,B) *Mef2*-driven overexpression of three independent UAS-*NUAK* lines result in smaller pupae (A) and adults (B) compared to controls. Scale bar, 1 mm. (C) Western blot shows that increasing levels of NUAK protein are produced in *mef2>NUAK 548* and *mef2>NUAK 550* compared to *mef2>NUAK EY*. ATP5α is used as a loading control to quantitate the relative amounts of NUAK protein in each genotype (bar graph). (D) Reduced organismal size is observed upon overexpression of the weaker *NUAK EY* line in muscle tissue (*mef2* and *24B*), but not in fat body (*ppl* and *cg*). Letters indicate significant differences between genotypes ($p < 0.05$).

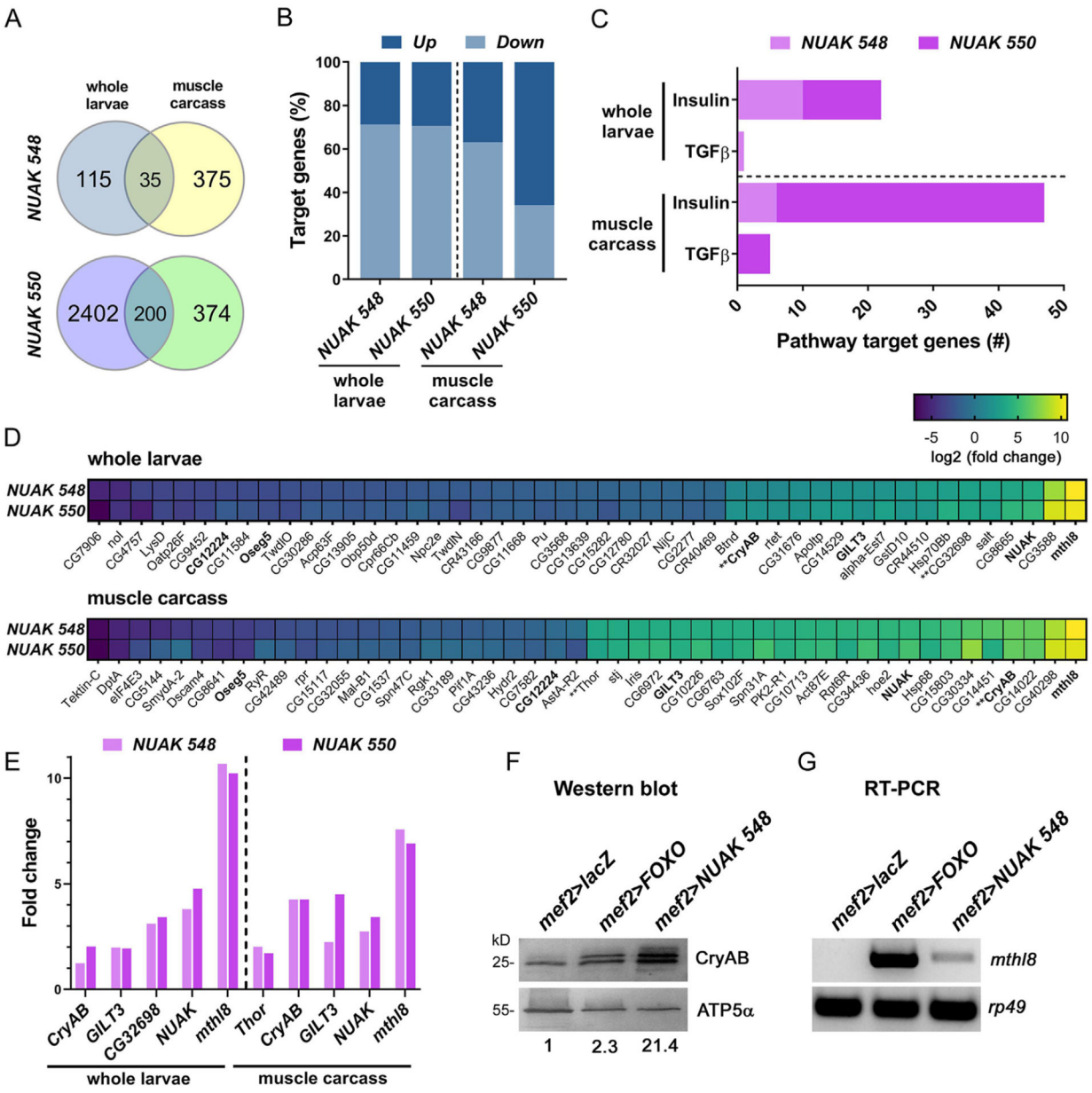

Fig. 2. RNA seq analysis reveals that muscle-expressed NUAK preferentially alters gene expression of insulin pathway targets.

(A) Venn diagram depicting the number of common genes detected in whole larvae and/or muscle carcass in *mef2>NUAK 548* vs. *mef2>lacZ* (top panel) or *mef2>NUAK 550* vs. *mef2>lacZ* (bottom panel). (B) Bar graph illustrates the relative percentage of up/down-regulated genes in whole larvae compared to muscle carcass upon *NUAK OE*. (C) Enrichment of insulin pathway target genes compared to target genes associated with TGFβ signaling in muscles expressing *NUAK*. (D) Heatmap depicting relative fold change (log_2) of the top up- or down-regulated genes detected in whole larvae (top panel) or muscle carcass (bottom panel) in *mef2>NUAK 548* or *mef2>NUAK 550* compared to *mef2>lacZ* controls. Gene names in bold are common between whole larvae and muscle carcass data sets. ** indicates known insulin pathway target genes. (E) Bar graph showing the relative

fold change of shared gene targets (*CryAB, GILT3, NUAK, mthl8*) and/or known insulin pathway targets (*CryAB, CG32698, Thor*) upon *NUAK OE*. (F) Western blot confirming upregulation of CryAB protein after expression of either *FOXO* or *NUAK 548* in muscle tissue. Relative fold change is indicated below the ATP5α blot, which was used as a loading control. (G) RT-PCR of *mthl8* transcript is undetectable in *mef2>lacZ* larvae, but is present in *mef2>FOXO* or *mef2>NUAK 548* larvae. *rp49* is used as a control.

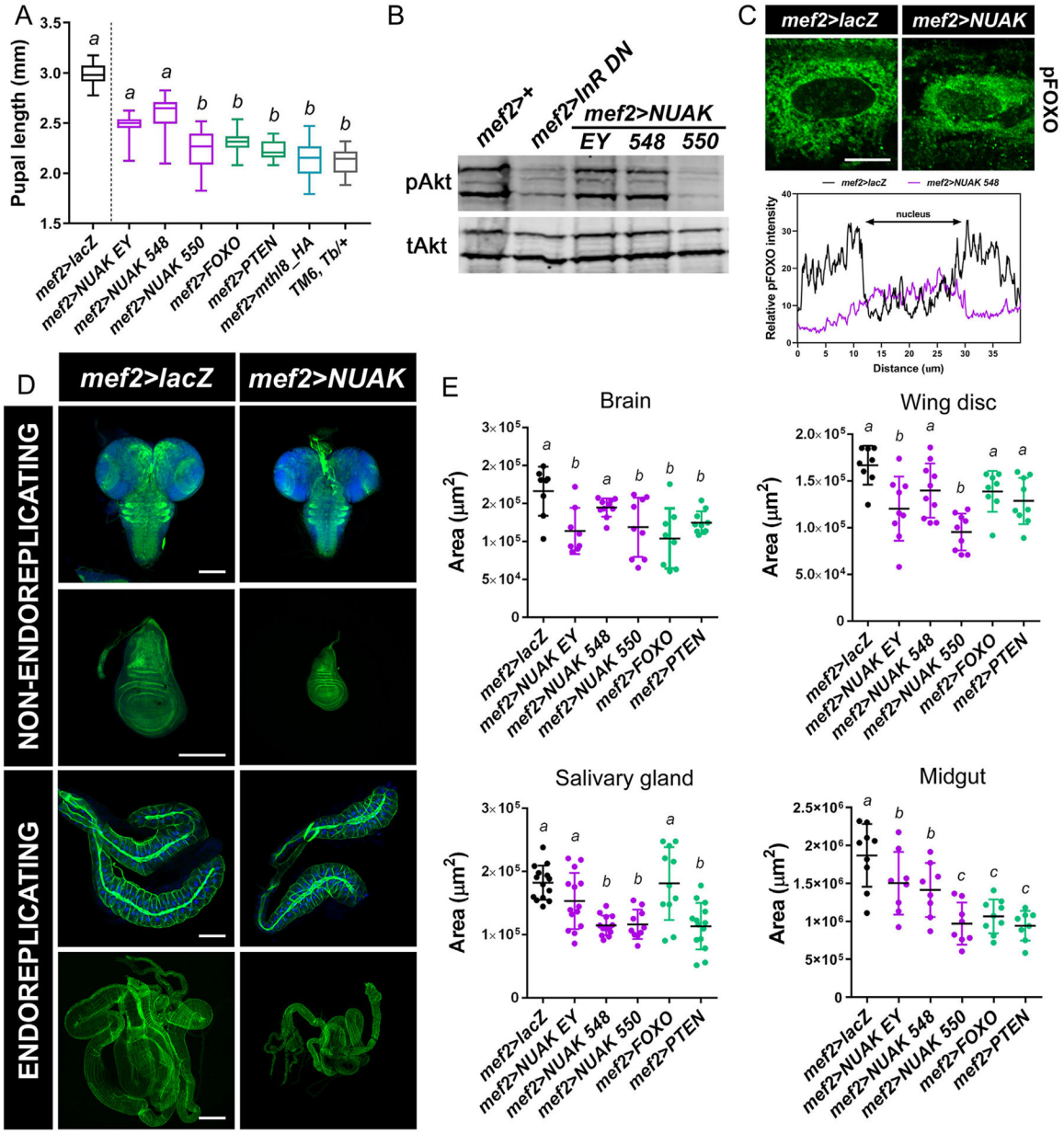

Fig. 3. NUAK OE phenocopies loss of insulin pathway outputs.

(A) Box and whisker plot reveals that *mef2*-induced *NUAK OE* or reduced insulin signaling reduces pupal size. This phenotype is also evident upon overexpression of *mef2>mthl8_HA*. The well characterized Tb mutation, present on a TMB balancer chromosome, was used as a control for small body size. (B) Western blot using pAkt (top panel) as a readout of insulin pathway activity. Expression of *mef2>InR DN* or *mef2>NUAK 550* abolishes activated pAkt signal, while total Akt protein levels are unchanged (bottom panel). (C) Single section confocal images of pFOXO staining. pFOXO is pre-dominantly localized in the cytoplasm in *mef2>lacZ* control larval muscle, but translocates to the nucleus upon *NUAK OE* for the activation of FOXO target genes. Scale bar, 10 µm. Line plot depicts the average relative intensity of pFOXO immunoreactivity corresponding to a 40 µm distance

that spans individual nuclei (n = 10 for each genotype). (D) Representative maximum intensity projections of larval non-endoreplicating (brain and wing disc) or endoreplicating (salivary gland and midgut) tissues from *mef2>lacZ* or *mef2>NUAK 548* animals stained with DAPI (blue) and F-actin (green). Scale bar, 100 μm. (E) Quantitation of the area of individual larval tissues. Expression of *NUAK* or negative regulators of insulin signaling (*FOXO* or *PTEN*) in muscle tissues generally reduced the size of all tissues examined compared to that of control *mef2>lacZ*. For all graphs, letters indicate significant differences between genotypes ($p < 0.05$).

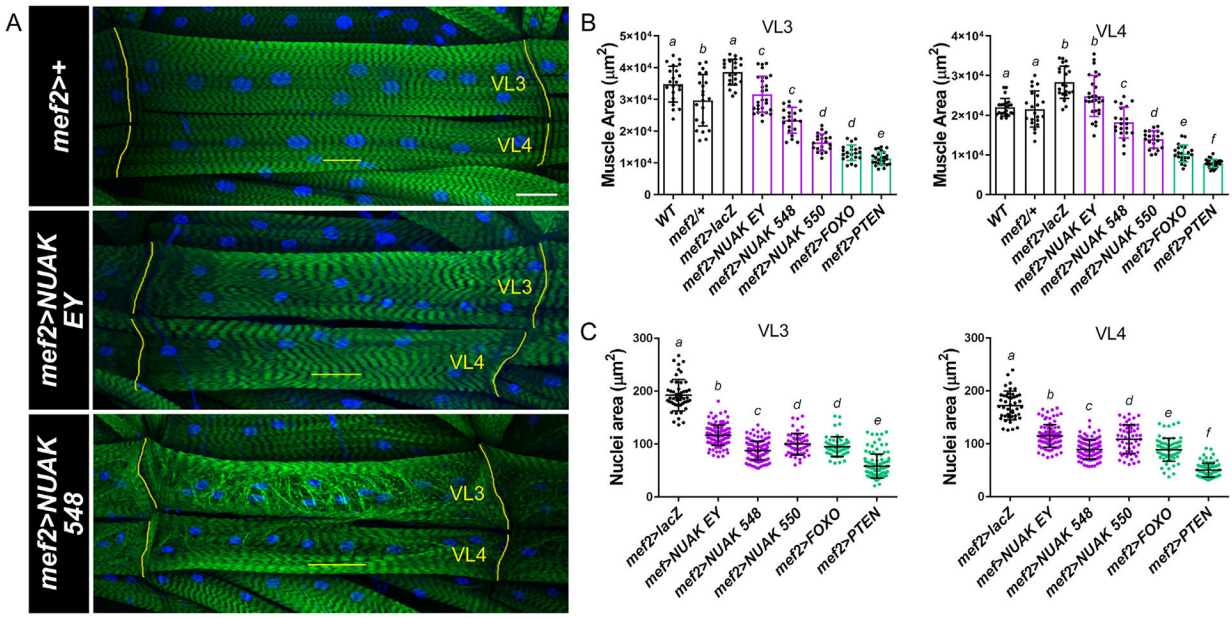

Fig. 4. Overexpression of NUAK or blunted insulin signaling reduces overall muscle size.

(A) Maximum intensity confocal images of VL3 and VL4 larval muscles in controls (top panel) or upon expression of *NUAK EY* (middle panel) or *NUAK 548* (bottom panel). Scale bar, 50 μm. (B) Scatter bar plot quantitation of VL3 (left panel) or VL4 (right panel) muscle area shows a graded reduction in muscle size upon *NUAK OE* or upon a block in insulin signaling (*FOXO* or *PTEN*). (C) Consistent with a reduction in muscle size, nuclei size is also reduced in VL3 muscles (left panel) and VL4 muscles (right panel) for all *mef2>NUAK OE* lines or in *mef2>FOXO* and *mef2>PTEN* larvae. For all graphs, Letters indicate significant differences between genotypes ($p < 0.05$).

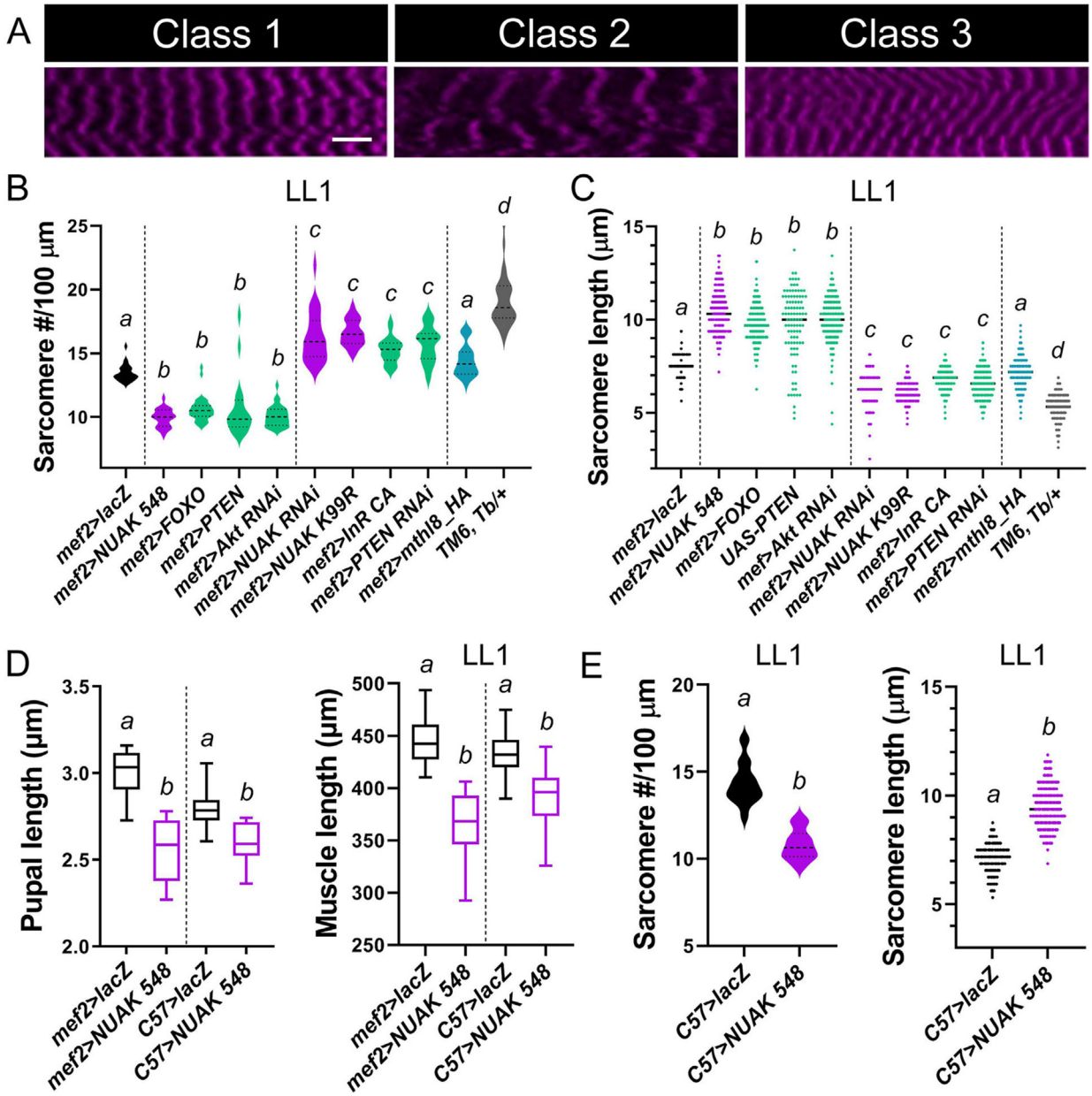

Fig. 5. Sarcomere alterations result from blocking or activating insulin signaling.

(A) Single plane images of larval LL1 muscles where the Z-discs of sarcomeres are marked with anti-Sls. Representative genotypes used for images are *mef2>lacZ* (Class 1), *mef2>NUAK 548* (Class 2), or *mef2>NUAK RNAi* (Class 3). Scale bar, 10 µm. (B,C) Violin plot (B) or scatter plot (C) of the indicated genotypes. (B) Control larvae possess ~12 sarcomeres/100 µm. Overexpression of *NUAK* or loss of insulin signaling reduces the average number of sarcomeres to ~10. Conversely, loss of *NUAK* function or activation of insulin pathway activity causes an increase in sarcomere number/100 µm. (C) The trend for sarcomere length is opposite that of sarcomere number. Insulin activation causes wider sarcomeres, while blocking insulin decreases sarcomere length. (D) *mef2* or *C57* expression of UAS-*NUAK 548* both cause smaller pupal body size (left panel) and reduced muscle

length (right panel). (E) Overexpression of *NUAK 548* during larval growth reduces the relative number of sarcomeres (left panel) and increases sarcomere length (right panel). For all graphs, Letters indicate significant differences between genotypes ($p < 0.05$).

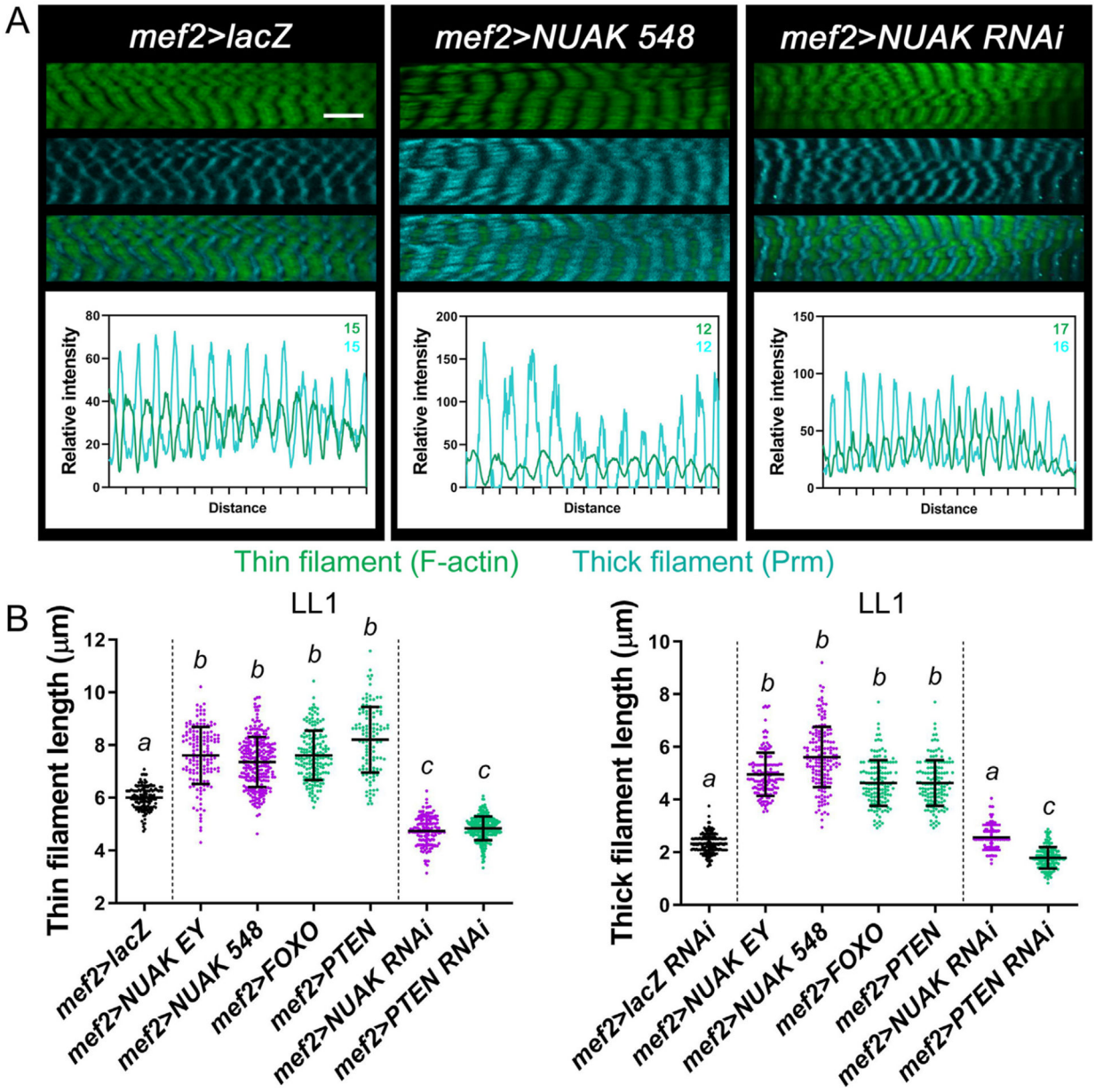

Fig. 6. Thin and thick filament lengths are coordinately regulated.

(A) Single plane confocal images of muscles from *mef2>NUAK 548* or *mef2>NUAK RNAi* individuals show differences in the lengths of thin filaments (F-actin, green) and thick filaments (Prm, cyan) compared to *mef2>lacZ* controls. Scale bar, 10 μm. (B) Scatter plots of thin filament (left panel) and thick filament (right panel) lengths of the indicated genotypes. Letters indicate significant differences between genotypes ($p < 0.05$).

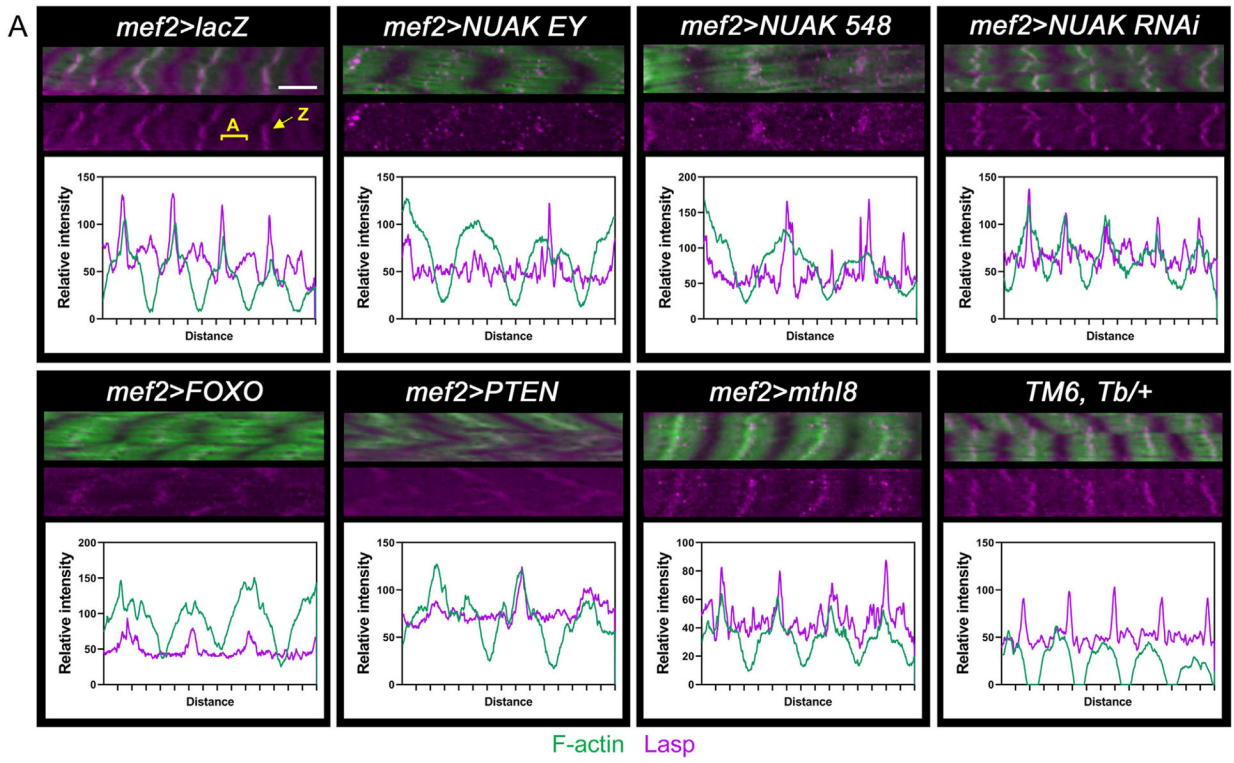

Fig. 7. Abnormal Lasp localization may account for sarcomere alterations.

(A) Representative single plane images showing F-actin (green) and Lasp (magenta) localization. The normal distribution of Lasp is altered upon *NUAK OE* or upon a block in insulin activity concomitant with wider sarcomeres (marked by F-actin). The relative localization of Lasp is restored in *mef2>NUAK RNAi* and *mef2>PTEN RNAi* muscles. Line plots indicate relative intensities of F-actin (green) and Lasp (magenta) across a fixed distance. Scale bar, 10 μm.